

# Scientifically-Interpretable Reasoning Network (SciReN): Discovering Hidden Relationships in the Carbon Cycle and Beyond

Joshua Fan<sup>\*1</sup>, Haodi Xu<sup>\*2</sup>, Feng Tao<sup>\*3</sup>, Md Nasim<sup>1</sup>, Marc Grimson<sup>1</sup>, Yiqi Luo<sup>2</sup>, Carla P. Gomes<sup>1</sup>

<sup>1</sup> Cornell University, Department of Computer Science

<sup>2</sup> Cornell University, School of Integrative Plant Science, Soil and Crop Sciences Section

<sup>3</sup> Cornell University, Department of Ecology and Evolutionary Biology

{jyf6,hx293,feng.tao,mn637,mg2422,yl2735}@cornell.edu, gomes@cs.cornell.edu

## Abstract

Understanding how carbon flows through the soil is crucial for mitigating the effects of climate change. While soils have potential to sequester carbon from the atmosphere, the soil carbon cycle remains poorly understood. Scientists have developed mathematical *process-based* models of the soil carbon cycle based on existing knowledge, but they contain numerous unknown parameters that must be set in an ad-hoc manner, and often fit observations poorly. On the other hand, neural networks can learn patterns from data, but do not respect known scientific laws, nor can they reveal novel scientific relationships due to their black-box nature. We thus propose *Scientifically-Interpretable Reasoning Network (SciReN)*, a fully-transparent framework that combines interpretable neural and process-based reasoning. An interpretable encoder predicts *scientifically-meaningful latent parameters*, which are then passed through a differentiable process-based decoder to predict labeled output variables. SciReN leverages Kolmogorov-Arnold networks (KAN) to ensure the encoder is fully interpretable and reveals relationships between input features and latent parameters; it uses novel smoothness penalties to balance expressivity and simplicity. SciReN also uses a novel hard-sigmoid constraint layer to restrict latent parameters to meaningful ranges defined by scientific prior knowledge. While the process-based decoder enforces established scientific knowledge, the KAN-based encoder reveals new scientific relationships hidden in conventional black-box models. We apply SciReN on two tasks: simulating the flow of organic carbon through soils, and modeling ecosystem respiration from plants. In both tasks, SciReN outperforms black-box networks in predictive accuracy while providing substantial scientific interpretability – it can infer latent scientific mechanisms and their relationships with input features.<sup>1</sup>

## 1 Introduction

Climate change poses major challenges to humanity, such as sea level rise, damages to agricultural production, and increased natural disasters (Lee et al. 2023). A potential way to slow global warming is by sequestering carbon from the atmosphere into the soil (Lal, Negassa, and Lorenz 2015). Soils play a crucial role in the global carbon cycle – they store more carbon than plants and the atmosphere combined

(Jobbágy and Jackson 2000). Yet it is difficult to understand how carbon flows through the soil, leading to high uncertainties in future climate projections (Luo et al. 2016).

Out of the box, neural networks can predict the total amount of organic carbon stored in the soil at each location (Tan et al. 2024). However, neural networks do not respect prior scientific knowledge about the carbon cycle – they can even produce predictions that violate basic scientific laws like mass conservation (Karpatne, Kannan, and Kumar 2022). Also, scientists want to *understand* the biogeochemical processes governing the soil carbon cycle – which control how much carbon can be stored in the soil and how long it will remain sequestered there. However, the black-box nature of neural networks makes it challenging to translate their predictive ability into novel scientific insights (Marcinkevičs and Vogt 2023).

To gain insight into these biogeochemical processes, ecologists have meticulously developed process-based models to simulate the soil carbon cycle (Luo and Smith 2022). These models are highly sophisticated, and may contain hundreds of pools representing different types of carbon, and matrices specifying flux rates between each pair of pools (Luo et al. 2022; Huang et al. 2018; Lu et al. 2020). However, these models contain many unknown parameters, which traditionally must be tuned by human experts through an inefficient trial-and-error process (Luo and Schuur 2020). These models often cannot fit observed data well, especially in cross-scale predictions, due to a poor understanding of the relationships between environmental conditions and parameter values. This is a key bottleneck in using process-based models for verifiable predictions on the global soil carbon cycle and its response to climate change.

A few prior works in hydrology (Tsai et al. 2021; Feng et al. 2022), phenology (van Bree, Marcos, and Athanasiadis 2025), ecosystem modeling (Reichstein et al. 2022), and soil biogeochemistry (Xu et al. 2025) have proposed implementing process-based models in a differentiable way so that poorly-understood parameters can be optimized by back-propagation or replaced with neural networks. While these approaches aim to combine process-based models with deep learning, the neural network components remain too opaque for scientists to understand, which leaves the relationships

<sup>\*</sup>These authors contributed equally.

<sup>1</sup>Preprint. Under review.

between the latent parameters and input features unclear.

To address these limitations, we propose a *Scientifically-Interpretable Reasoning Network (SciReN)*, an end-to-end differentiable framework that embeds scientific process-based models into a *fully-transparent* neural model, creating a system that respects scientific knowledge, learns from data in an end-to-end manner, and can discover new scientific relationships. SciReN contains three main components. First, a learnable encoder takes in environmental features for a given location, and predicts scientifically-meaningful latent parameters. We use a *fully-interpretable model* such as a sparse Kolmogorov-Arnold network (Liu et al. 2024c) to make this portion fully transparent, allowing scientists to understand the relationships between latent parameters and input features. Second, a hard-sigmoid constraint layer projects these parameters into a physically-plausible range set by prior knowledge. Finally, a process-based decoder uses these predicted parameters to simulate the flow of carbon through the soil based on scientific knowledge, and finally predicts the output variables (e.g. amount of organic carbon at each depth in the soil). We compare the predicted outputs with ground-truth labels, and backpropagate this loss to train the entire system.

**Our main contributions are:** (1) We propose a *fully-interpretable* framework for combining scientific reasoning (in the form of process-based modeling) with data-driven learning. Unlike prior work, our model is able to infer *unobserved physical processes*, and reveal their relationships to input variables in a fully-transparent way. (2) We balance smoothness and expressivity in the learned functional relationships by using B-splines with novel smoothness penalties. (3) We propose a novel hard-sigmoid constraint layer to constrain the scientific parameters to fall within physically-plausible ranges. (4) We validate our technique on two scientific domains. First, we apply SciReN on a model of ecosystem respiration; SciReN discovers the correct relationships between latent parameters and input features, while other methods do not. It also improves out-of-distribution extrapolation compared to black-box models. Second, we test SciReN on the challenging task of modeling the soil carbon cycle, where we need to simulate carbon flows through 140 soil pools at each location. On a synthetic dataset, SciReN is able to predict *unlabeled* latent biogeochemical parameters and accurately retrieve their relationships with environmental features. With real data, SciReN simulates observed soil carbon amounts with accuracy comparable to blackbox methods. We hope our work inspires other researchers to apply and extend SciReN across diverse scientific tasks, advancing AI’s capacity for interpretable scientific discovery.

## 2 Related work

**Knowledge-Guided Machine Learning.** There is a rich history of incorporating prior knowledge into neural networks by modifying the loss function, pretraining procedure, or model architecture (Karpatne, Jia, and Kumar 2024; Willard et al. 2022). A simple approach is to add a loss term that penalizes when physical laws are violated (Daw et al. 2022; Beucler et al. 2019; Jia et al. 2019). For example, the density of water is known to increase monotonically with

depth; thus, Daw et al. (2022) and Jia et al. (2019) use a “monotonicity loss” that penalizes when the model’s predictions are not monotonic. Physics-informed neural networks assume that the governing equation of a system is known, and penalize when its predictions and gradients violate this equation (Raissi, Perdikaris, and Karniadakis 2019), but are hard to train (Krishnapriyan et al. 2021; Rathore et al. 2024). Process-based models can be used to generate synthetic data to pretrain the network (Jia et al. 2021; Liu et al. 2024a). Overall, while these approaches use prior knowledge to guide the model, they cannot guarantee that physical constraints will be satisfied (Willard et al. 2022), and cannot easily provide new insights into physical processes.

One can also design model architectures to encode prior knowledge. Convolutional neural networks encode inductive biases such as translation equivariance and locality into the model architecture, reducing the amount of training data required to classify images (LeCun, Bengio et al. 1995). In lake temperature modeling, Daw et al. (2020) design a monotonicity-preserving LSTM that produces monotonically-increasing intermediate variables (densities) by design. In agriculture, Liu et al. (2024a) design a hierarchical neural network that incorporates causal relations between different variables. However, it is difficult to design a new architecture for every problem.

**Combining reasoning and learning.** A few works reason about constraints and prior knowledge within the network itself. Deep Reasoning Networks use entropy-based losses to encourage the latent space to be interpretable and satisfy constraints (e.g. in Sudoku, each row must contain exactly one of each number) (Chen et al. 2020). This approach was used to solve the phase-mapping problem in materials discovery, where the constraints are thermodynamic rules (Chen et al. 2021). CLR-DRNets enhanced the reasoning process using a modified LSTM, and used curriculum learning to improve trainability (Bai, Chen, and Gomes 2021). Physically-informed Graph-based DRNets add a physical decoder that reconstructs X-ray diffraction patterns based on Bragg’s law (Min et al. 2023). CS-SUNet encourages pixels with similar input features to have similar predictions, enabling weakly-supervised prediction (Fan et al. 2022). While these models have an interpretable latent space, the bulk of the network remains uninterpretable.

**Process-based models.** Scientists develop *process-based models* to simulate physical processes based on domain knowledge (Cuddington et al. 2013). These models consist of mathematical equations that describe the relationships between various variables. In soil science, *pool-and-flux* models are common, where a matrix equation tracks the amount of carbon at each soil depth and matter type (Luo and Smith 2022). Transition matrices encode the rate at which carbon is transferred between pools, which are functions of soil and climate properties. Many scientific models can be unified under this matrix form (Huang et al. 2018; Luo et al. 2022).

Unfortunately, despite their sophistication, these models have difficulty matching real observations, and have numerous unknown parameters that are traditionally set in an ad-hoc way. These unknown parameters need to vary across

space and (sometimes) time, but are difficult to estimate (Luo and Schuur 2020). A state-of-the-art approach for setting these parameters is PRODA (Tao et al. 2020). PRODA first runs Bayesian data assimilation at each location separately to find optimal biogeochemical parameters for each location. Then, a neural network is trained to predict these optimal parameters given environmental covariates. While this approach is effective, it is computationally expensive, and is not always robust since each location’s parameters are estimated with only a few observations.

**Differentiable Process-Based Models.** A few works integrate process-based models and neural networks in an end-to-end differentiable framework; this has been called *differentiable parameter learning* (Tsai et al. 2021), *hybrid modeling* (Reichstein et al. 2022), or *differentiable process-based modeling* (Shen et al. 2023). For example, (van Bree, Marcos, and Athanasiadis 2025; Reichstein et al. 2022; Tsai et al. 2021) used a process-based model as the main backbone, but replaced some poorly-understood components with neural networks. By implementing the process-based model in a differentiable way, the model could be trained end-to-end, and unknown components could be fit using data. Xu et al. (2025) scaled this approach up to a more complex soil carbon model with 21 unknown parameters and 140 carbon pools. However, the neural network component is still opaque, making it difficult for scientists to discover new relationships and insights.

**Explainable and Interpretable AI.** A subfield of machine learning aims to interpret how neural networks make predictions (Molnar 2025). *Post-hoc feature attribution methods* such as SHAP (Lundberg and Lee 2017) or Integrated Gradients (Sundararajan, Taly, and Yan 2017) estimate the impact of each feature on the model’s prediction for a given example. *Local surrogate models* such as LIME (Ribeiro, Singh, and Guestrin 2016) fit an interpretable surrogate model that approximates the black-box model in a small area, but it is hard to infer global behavior from local approximations. *Marginal effect plots* such as Partial Dependence Plots (Friedman 2001) or Accumulated Local Effects plots (Apley and Zhu 2020) visualize how each feature affects the output on average. These methods are mere approximations of a black-box model, and can produce misleading explanations if the approximation is poor (Rudin 2019).

On the other hand, *inherently-interpretable models* aim to make the entire model transparent by design (Rudin 2019). In linear regression, coefficients precisely reveal how each input affects the prediction. Unfortunately, linear models are often not expressive enough. Neural additive models add expressivity by modeling the output variable as the sum of single-variable functions (one for each input) (Agarwal et al. 2021). However, they cannot represent complex interactions between variables. Kolmogorov-Arnold networks stack multiple additive models into layers, and are universal approximators in theory (Liu et al. 2024c). All of these approaches are typically applied in supervised settings – they have not been combined with process-based models or scientific knowledge to predict *unlabeled* variables.

### 3 Methods

To combine scientific knowledge and data-driven learning into a fully-transparent model, SciReN contains three main components. First, a neural network encoder  $f_{NN}$  (with learnable weights  $\theta$ ) takes in input features  $\mathbf{x} \in \mathbb{R}^D$  (e.g. soil and climate variables at a given location), and outputs unconstrained latent parameters  $\mathbf{a} \in \mathbb{R}^P$ :  $\mathbf{a} = f_{NN}(\mathbf{x}; \theta)$ . In SciReN,  $f_{NN}$  should be fully-transparent, which can be achieved by making it a neural additive model or sparse Kolmogorov-Arnold network. The latent parameters are scientifically-meaningful variables that govern the underlying physical process, yet cannot be observed directly. Secondly, a constraint layer maps the unconstrained parameters to a scientifically-plausible prior range for each parameter set by prior knowledge;  $\mathbf{p} = \text{Proj}(\mathbf{a})$ . Finally, the constrained parameters are passed through a *fixed, deterministic* process-based decoder  $g_{PBM}$ , which simulates the system and produces the final predicted output  $\hat{y} = g_{PBM}(\mathbf{p})$ . We compare this with the true label and backpropagate. The framework is summarized in Figure 1, and we elaborate on each component below.

#### 3.1 Encoder: Learned Interpretable Relationships

We want to learn a function  $f_{NN}$  mapping observed input features  $\mathbf{x}$  to latent scientific parameters  $\mathbf{p}$ . In prior work, this function is typically a fully-connected neural network (Xu et al. 2025; van Bree, Marcos, and Athanasiadis 2025; Reichstein et al. 2022; Tsai et al. 2021). However, scientists want to understand how biogeochemical parameters (e.g. transfer rates between pools) depend on input features (e.g. temperature); neural networks do not provide these insights.

Recently, a line of work has aimed to produce neural networks that are inherently interpretable while being expressive. Neural additive models (NAM) (Agarwal et al. 2021) model the output as the sum of single-variable functions of each input feature. Specifically, they learn a neural network  $\phi_i : \mathbb{R} \rightarrow \mathbb{R}$  (with one input and one output) for each feature  $x_i$ , and sum contributions from each feature into the output:

$$NAM(\mathbf{x}) = b + \sum_{i=1}^D \phi_i(x_i; \theta_i) \quad (1)$$

where  $(b, \{\theta_i\}_{i=1}^D)$  are learnable parameters trained via backpropagation. While NAM is quite expressive, it cannot model non-additive feature interactions, which are important in soil science (Dieleman et al. 2012).

To increase the expressivity of neural additive models, we can generate intermediate variables using neural additive model of the inputs, then further use a neural additive model on the intermediate variables to generate the output. Specifically, generate intermediate variables  $\mathbf{z} = \{z_1, \dots, z_H\}$  as

$$z_j = NAM_j(\mathbf{x}) = b_j + \sum_{i=1}^D \phi_{j,i}(x_i), \quad \forall j \in [1, H] \quad (2)$$

Now define each output variable  $a_p$  as a neural additive

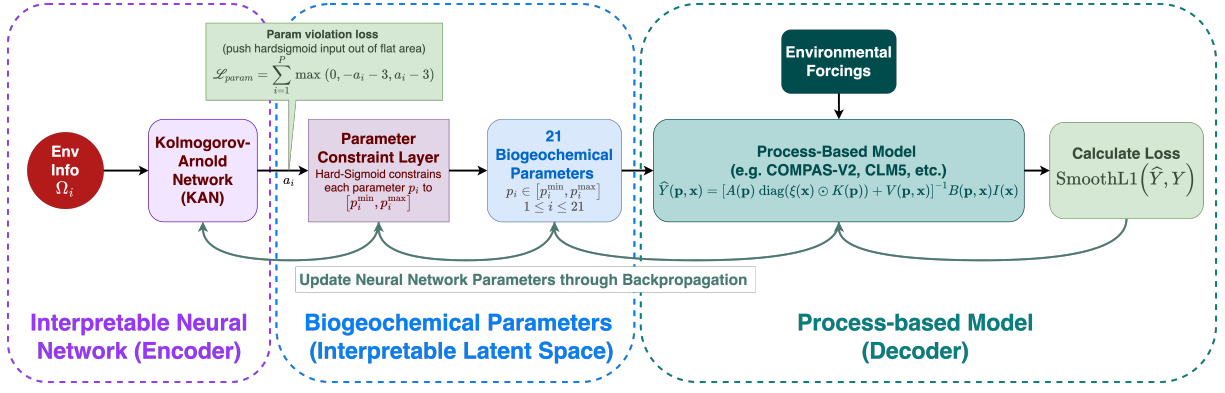


Figure 1: Overview of SciReN. The encoder is a fully-interpretable model that reveals functional relationships between input features and latent scientific parameters. A constraint layer forces the latent parameters to be within a pre-specified range, and the process-based decoder uses the predicted latent parameters to simulate the physical process and predict the final output.

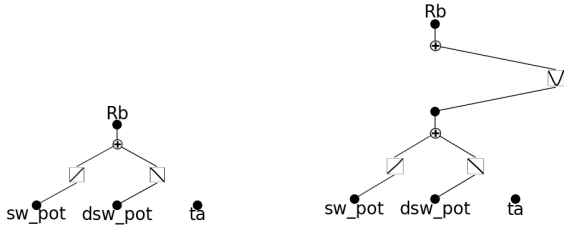


Figure 2: Learned encoder examples: 1-layer KAN (left) and 2-layer KAN (right)

model over the intermediate variables

$$a_p = NAM_p(\mathbf{z}) = b_p + \sum_{j=1}^H \Phi_{p,j}(z_j) \quad (3)$$

$$= b'_p + \sum_{j=1}^H \Phi_{p,j} \left( \sum_{i=1}^D \phi_{j,i}(x_i) \right) \quad (4)$$

where all the bias terms are collected into  $b'_p$ . This is now the same form as a two-layer Kolmogorov-Arnold network (KAN, see equation 2.1 in (Liu et al. 2024c)). By the Kolmogorov-Arnold theorem, this multi-layer stack of neural additive models can approximate any multivariate continuous function (Liu et al. 2024c).

Two examples of learned encoders are shown in Figure 2. On the left, a 1-layer KAN models the latent parameter  $Rb \approx w_1 \cdot sw\_pot + (-w_2) \cdot dsw\_pot$ . One can immediately see how each feature influences  $Rb$ . On the right, a 2-layer KAN is needed to capture this nonlinear relationship, where an intermediate variable  $Rb' \approx w_1 \cdot sw\_pot + (-w_2) \cdot dsw\_pot$ , and then  $Rb \approx |Rb'|$ .

### 3.2 Sparsity and Smoothness Regularization

Kolmogorov-Arnold networks are still hard to interpret if each output depends on many inputs. Liu et al. (2024b) propose entropy regularization to sparsify the network. Specifically, we compute an importance score for each edge, as

the mean absolute deviation of the output activations from the edge, weighted by their eventual contribution to the final output variables (Liu et al. 2024b); see Appendix for details. We denote this score for edge  $(i \rightarrow j)$  in layer  $l$  as  $E_{i,j}^l$ . We encourage the entropy of the edge importance distribution to be low (making the network choose a few important edges and push others towards zero). We also encourage the absolute deviation of each edge’s outputs to be low via an L1 penalty:

$$e_{i,j}^l = \frac{E_{i,j}^l}{\sum_{i',j'} E_{i',j'}^l} \quad (\text{normalize edge importance to sum to 1}) \quad (5)$$

$$\mathcal{L}_{entropy} = - \sum_l \sum_{i,j} e_{i,j}^l \log e_{i,j}^l; \quad \mathcal{L}_{L1} = - \sum_l \sum_{i,j} |E_{i,j}^l| \quad (6)$$

Note that KANs parameterize the learnable edge activation functions  $\Phi, \phi$  using B-splines instead of neural networks. B-splines represent a curve as a weighted sum of basis functions, each of which peaks at a different point on the x-axis (see (Eilers and Marx 1996) for details). We can apply a second-order difference penalty on the spline coefficients – this encourages the coefficients to change in a linear way, making the function more linear (Eilers and Marx 2010). To our knowledge this has not been proposed with KANs before; this allows us to increase the number of basis functions (knots) and the function’s expressivity while maintaining smoothness and preventing overfitting. If  $c_1 \dots c_G$  are the coefficients, the penalty is

$$\mathcal{L}_{smooth} = \sum_{i=1}^{G-2} ((c_{i+2} - c_{i+1}) - (c_{i+1} - c_i))^2 \quad (7)$$

### 3.3 Linear Parameter Constraint Layer

For some latent scientific parameters  $p_i$ , there is a known prior range  $[p_i^{min}, p_i^{max}]$  based on prior knowledge and physical plausibility. Xu et al. (2025) applied a sigmoid function to the encoder output  $a_i$  to force the predicted parameter into the prior range:  $p_i = \sigma(a_i)$ . However, this adds

### Hard-Sigmoid Activation Parameter Violation Loss

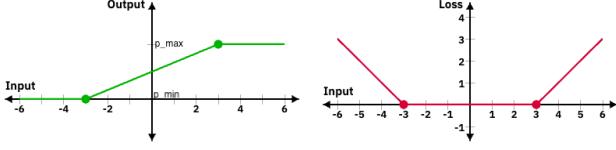


Figure 3: **Left:** The hard-sigmoid function constrains parameters to  $[p_{min}, p_{max}]$ , without adding nonlinearity. **Right:** parameter violation loss pushes the hard-sigmoid input away from flat regions.

nonlinearity and harms interpretability. For example, suppose a parameter  $p_i$  is actually a linear function of input variable  $x_j$ ,  $p_i = wx_j$ . If the parameter was constrained using a sigmoid, the unconstrained encoder would have to learn  $a_i = \sigma^{-1}(wx_j)$ , so that after the sigmoid function the parameter becomes  $p_i = \sigma(\sigma^{-1}(wx_j)) = wx_j$ . The additional inverse sigmoid makes the function less interpretable.

Instead, we use a piecewise linear *hard-sigmoid* function (Figure 3 left) to constrain the parameters:

$$p_i = \begin{cases} p_i^{min} & \text{if } a_i \leq -3, \\ p_i^{max} & \text{if } a_i \geq 3, \\ \frac{p_i^{max} - p_i^{min}}{6} \cdot a_i + \frac{p_i^{max} + p_i^{min}}{2} & \text{otherwise} \end{cases} \quad (8)$$

While the gradient  $\frac{\partial p_i}{\partial a_i}$  is zero when  $a_i$  is outside the range  $[-3, 3]$ , we can add another loss that places a penalty when  $a_i$  is in the flat area (figure 3 right).

$$\mathcal{L}_{param} = \sum_{i=1}^P \max(0, -a_i - 3, a_i - 3) \quad (9)$$

This provides a gradient that pushes  $a_i$  towards the linear range  $[-3, 3]$  when it is in the flat range.

For the ecosystem respiration model, we only know that the latent parameter is nonnegative, so we use ReLU to impose the constraint, and a flipped ReLU loss to push inputs out of the flat region.

$$p_i = \max(a_i, 0); \quad \mathcal{L}_{param} = \max(-a_i, 0) \quad (10)$$

### 3.4 Differentiable Process-Based Decoder

SciReN uses a process-based model that expresses output variables as a *fixed, differentiable function* of scientific parameters and input variables:  $\hat{y} = g_{PBM}(\mathbf{p}, \mathbf{x})$ . Two examples are described below.

**Ecosystem respiration.** Consider the model of ecosystem respiration in (Reichstein et al. 2022). Based on scientific knowledge, we write the output variable  $R_{eco}$  (ecosystem respiration) as a differentiable function of two latent parameters, base respiration  $R_b$  and temperature sensitivity  $Q_{10}$ :

$$R_{eco} = g_{PBM}(\mathbf{p}, \mathbf{x}) = R_b(\mathbf{x}) \cdot Q_{10}^{\frac{t_a - T_{ref}}{10}} \quad (11)$$

where the latent parameters are  $\mathbf{p} = \{R_b, Q_{10}\}$ , the input features are  $\mathbf{x} = \{sw\_pot, dsw\_pot, t_a\}$ , and  $T_{ref} = 15$ .  $R_b$  has an unknown relationship with the input features (learned in the encoder), while  $Q_{10}$  is a learnable constant.

**Soil carbon modeling.** As a more complex process, we use the soil organic carbon module from Community Land Model 5 (CLM5) (Lu et al. 2020), which tracks the amount of soil organic carbon (SOC) in 140 pools in the soil (20 depths and 7 material types per depth). Denote the amount of carbon in pool  $i$  as  $Y_i$ . The core of the model is a mass conservation equation for each pool, where the change in carbon equals inflow (from plants and other pools) minus outflow (to other pools or the atmosphere):

$$\frac{dY_i(t)}{dt} = \text{inflow to pool } i - \text{outflow from pool } i \quad (12)$$

The equations for each pool can be combined into a single matrix equation. If we assume steady state ( $\frac{dY_i(t)}{dt} = 0$ ), we can write  $Y$  as a function of biogeochemical parameters  $\mathbf{p}$  and input features  $\mathbf{x}$ :

$$\hat{Y}(\mathbf{p}, \mathbf{x}) = [A(\mathbf{p}) (\xi(\mathbf{x}) \odot K(\mathbf{p})) + V(\mathbf{p}, \mathbf{x})]^{-1} I(\mathbf{p}, \mathbf{x}) \quad (13)$$

The details of this equation are explained in the Appendix. For now, it is sufficient to note that the process-based model takes in 21 latent biogeochemical parameters  $\mathbf{p}$ , uses the parameters to construct matrices describing carbon fluxes and decomposition, and finally predicts the amount of carbon in 140 pools (20 layers and 7 pools),  $\hat{Y}$ . Each operation (including matrix inversion) is differentiable and can be implemented in PyTorch. Note that our labeled data only contains aggregate SOC amounts at specific depths (which may not match the 20 fixed layers). Thus, we sum up the SOC pools at each layer, and linearly interpolate to predict SOC at the observed depths.

### 3.5 Final Loss

The final loss contains a smooth L1 loss between the predicted and ground-truth output variables, as well as the parameter regularization loss and KAN regularization losses:

$$\mathcal{L} = \sum_{i=1}^N \left[ \text{SmoothL1}(\hat{Y}_i, Y_i) \right] + \lambda_{param} \mathcal{L}_{param} + \lambda_{L1} \mathcal{L}_{L1} + \lambda_{entropy} \mathcal{L}_{entropy} + \lambda_{smooth} \mathcal{L}_{smooth}$$

Since the entire network is differentiable, we can backpropagate the loss through the process-based model to optimize the latent parameters and the learnable weights of the neural network. The loss weights  $\lambda$  are tuned on a validation set for each domain; they are relatively intuitive to tune since we can visualize whether the KAN is too sparse/dense and whether the functions are too sparse/dense and whether the functions are too sparse/dense and whether the functions are too sparse/dense and whether the functions are too sparse/dense.

## 4 Experiments

We test our approach on two domains: the model of ecosystem respiration in (Reichstein et al. 2022), and the CLM5 soil carbon cycle model (Xu et al. 2025).

### 4.1 Evaluation Metrics and Baselines

For each dataset, we first verify that methods are able to predict observed variables, by measuring  $R^2$  on the test set.

However, the main novelty of SciReN is its ability to infer hidden functional relationships between input features and latent parameters. We thus conduct experiments on synthetic data to verify that SciReN infers the correct latent parameters and functional relationships. To evaluate functional relationship quality, for both ground-truth (synthetic) relationships and our learned models, we first compute the fraction of variance in the output that is explained by each input feature. For 1-layer KAN, we can simply compute the variance of each edge’s post-activation outputs, and divide by the total variance in the output. For other models, this is non-trivial; we use Partial Dependence Variance (Greenwell, Boehmke, and McCarthy 2018) to estimate how much variance in the output is explained by each input feature. Once we have feature importance distributions, we use KL divergence to measure how far the model’s learned feature importances are from the ground-truth.

For baselines, we compare against a pure neural network that only predicts observed variables (and cannot infer latent variables), and a blackbox hybrid model (Reichstein et al. 2022; Xu et al. 2025) where latent parameters are predicted by a neural network. We run SciReN and Blackbox-Hybrid using a nonlinear constraint (sigmoid or softplus) and a linear constraint (hard-sigmoid or ReLU).

## 4.2 Ecosystem Respiration

For ecosystem respiration, we used the same dataset and splits as (Reichstein et al. 2022), except we removed the 20% highest-temperature examples from the train set, forcing the model to extrapolate to higher temperatures than seen during training. We created two sets of latent  $R_b$  (base respiration) values. First, we model  $R_b$  as a linear function of 2 features  $sw\_pot$ ,  $dsw\_pot$  (as in Reichstein et al. (2022)):

$$R_b = 0.0075 \cdot sw\_pot - 0.00375 \cdot dsw\_pot + 1.03506858 \quad (14)$$

Second, to create a setting where a 2-layer KAN is needed, we add an absolute value.

$$R'_b = 0.0075 \cdot sw\_pot - 0.00375 \cdot dsw\_pot \quad (15)$$

$$R_b = \left| \frac{R'_b - \text{mean}(R'_b)}{\text{stdev}(R'_b)} \right| + 0.1 \quad (16)$$

We then generated the observed variable  $R_{eco}$  according to the process-based model with multiplicative noise, as in (Cohrs et al. 2024):

$$R_{eco} = R_b \cdot Q_{10}^{\frac{t_a - T_{ref}}{10}} \cdot (1 + \epsilon), \quad \epsilon \sim N(0, 0.1), \quad (17)$$

Table 1 shows results for the first setting (linear  $R_b$ ). For predicting the observed variable  $R_{eco}$ , Blackbox-Hybrid and SciReN outperform pure-NN as the process-based model provides prior knowledge that helps the model extrapolate out-of-distribution. For inferring the latent variable  $R_b$  and functional relationships, SciReN with linear constraint does best; it correctly learns that  $R_b$  only depends on  $sw\_pot$  and  $dsw\_pot$ , not  $t_a$  (see Figure 2 left). This is difficult because the irrelevant feature  $t_a$  (air temperature) is highly correlated with feature  $sw\_pot$ . Also, if the model learns the wrong  $Q_{10}$  value, it can make  $R_b$  depend on  $t_a$  to compensate. SciReN’s

entropy loss pushes it to eliminate as many variables as possible, and the smoothness loss (with the linear constraint) makes the relationship as linear as possible. Other methods learn complex relationships that perform worse.

Table 2 shows results for nonlinear  $R_b$ , where a 2-layer KAN is needed to model the complex relationship (1 layer is insufficient). SciReN predicts the observed variable, latent variable, and functional relationships almost perfectly, greatly outperforming pure-NN and Blackbox-Hybrid. Figure 2 (right) shows that SciReN learned the true relationship.

## 4.3 Soil carbon cycle

For soil carbon, we split the US into  $2 \times 2$  degree blocks and randomly assign the blocks to five folds, as in (Wang et al. 2020). We average across five data splits – each split uses one fold for testing, one for validation, and the other folds for training. Each split also uses its own initial seed.

First, we synthetically generate functional relationships between the 10 input features and 4 most sensitive biogeochemical parameters from (Xu et al. 2025). Of the  $10 \times 4 = 40$  possible relationships, we select 20% and randomly assign each to (linear, quadratic, log, exp, abs) with random affine shifts. We set the other parameters to default values as they are poorly constrained by data (Xu et al. 2025); this *equifinality* is an inherent limitation of process-based models, which we mitigate by only predicting the 4 most sensitive parameters. We then use the CLM5 process-based model to generate synthetic SOC labels from these parameters. Table 3 shows how various methods perform in recovering these functional relationships. SciReN (1-layer KAN) recovers the ground-truth relationships (see Figure 4) and observed/latent variables almost perfectly, while Blackbox-Hybrid is not incentivized to produce sparse relationships and mixes correlated features in.

Finally, we train all methods on real carbon labels in Table 4. SciReN’s accuracy in predicting SOC amounts is comparable to blackbox hybrid models and outperforms pure neural networks (in terms of  $R^2$ ). This indicates that we can obtain full interpretability without significantly sacrificing predictive accuracy. Note that a 1-layer KAN is enough to achieve good accuracy, making the encoder even easier to interpret. Scientists can examine the predicted relationships and check if they are consistent with current knowledge.

## 5 Conclusion

We have proposed SciReN, an end-to-end framework that combines data-driven learning with established scientific knowledge (in the form of process-based reasoning) to discover interpretable relationships between latent scientific parameters and inputs. The entropy loss helps the model discover robust relationships and disregard irrelevant variables, while the smoothness loss enables expressivity without overfitting. A limitation of SciReN is that the KAN encoder has many hyperparameters (including loss weights) which significantly impact performance; future work could pursue making KANs easier to train. Nevertheless, SciReN demonstrates excellent performance at retrieving true functional relationships, can extrapolate out-of-distribution, and contains

Table 1: Ecosystem respiration, linear  $R_b$ . Mean and standard deviation across 5 seeds.

Method	$R^2$ (observed, $\uparrow$ )	$R^2$ (latent, $\uparrow$ )	KL, functional relationships ( $\downarrow$ )
Pure-NN	$0.968 \pm 0.004$	N/A	N/A
Blackbox-Hybrid, nonlinear constraint	$0.972 \pm 0.003$	$0.818 \pm 0.052$	$0.284 \pm 0.041$
Blackbox-Hybrid, linear constraint	<b><math>0.976 \pm 0.001</math></b>	$0.941 \pm 0.031$	$0.161 \pm 0.068$
SciReN, nonlinear constraint (1-layer KAN)	$0.975 \pm 0.000$	$0.995 \pm 0.000$	$0.002 \pm 0.001$
SciReN, linear constraint (1-layer KAN)	<b><math>0.976 \pm 0.000</math></b>	<b><math>1.000 \pm 0.000</math></b>	<b><math>0.001 \pm 0.001</math></b>

Table 2: Ecosystem respiration, nonlinear  $R_b$ . Mean and standard deviation across 5 seeds.

Method	$R^2$ (observed, $\uparrow$ )	$R^2$ (latent, $\uparrow$ )	KL, functional relationships ( $\downarrow$ )
Pure-NN	$0.946 \pm 0.004$	N/A	N/A
Blackbox-Hybrid, nonlinear constraint	$0.948 \pm 0.008$	$-0.265 \pm 0.355$	$0.937 \pm 0.168$
Blackbox-Hybrid, linear constraint	<b><math>0.961 \pm 0.001</math></b>	$0.949 \pm 0.059$	$0.199 \pm 0.094$
SciReN, linear constraint (1-layer KAN)	$0.651 \pm 0.014$	$-1.225 \pm 0.668$	$1.182 \pm 0.085$
SciReN, linear constraint (2-layer KAN)	<b><math>0.961 \pm 0.001</math></b>	<b><math>0.993 \pm 0.005</math></b>	<b><math>0.078 \pm 0.045</math></b>

Table 3: Soil carbon cycle (synthetic parameters). Mean and standard deviation across 5 splits/seeds.

Method	$R^2$ (observed, $\uparrow$ )	$R^2$ (latent, $\uparrow$ )	KL, functional relationships ( $\downarrow$ )
Pure NN	$0.944 \pm 0.026$	N/A	N/A
Blackbox-Hybrid, nonlinear constraint	$0.997 \pm 0.001$	$0.491 \pm 0.155$	$0.878 \pm 0.127$
Blackbox-Hybrid, linear constraint	$0.997 \pm 0.001$	$0.558 \pm 0.142$	$0.864 \pm 0.141$
SciReN, linear constraint (1-layer KAN)	<b><math>1.000 \pm 0.001</math></b>	<b><math>0.999 \pm 0.000</math></b>	<b><math>0.046 \pm 0.018</math></b>

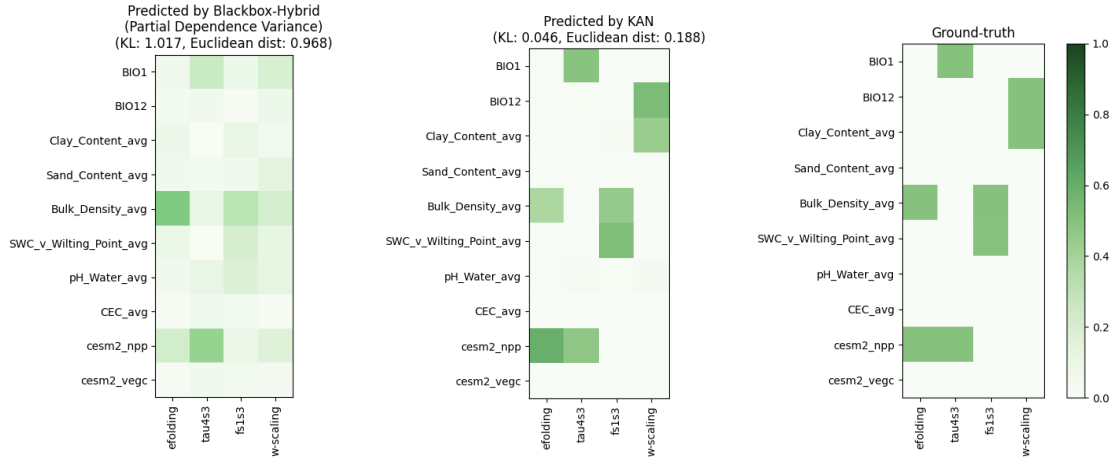


Figure 4: Functional relationships learned by Blackbox-Hybrid (left) and SciReN (center) vs. truth (right), on synthetic labels. SciReN recovers the true relationships much more accurately.

Table 4: Soil carbon cycle (real labels). Mean and standard deviation across 5 splits/seeds.

Method	$R^2$ ( $\uparrow$ )	MAE ( $\downarrow$ )	Pearson correlation ( $\uparrow$ )
Pure NN	$0.552 \pm 0.173$	<b><math>4609.3 \pm 356.8</math></b>	<b><math>0.780 \pm 0.053</math></b>
Blackbox-Hybrid, nonlinear constraint	$0.584 \pm 0.082$	$4726.2 \pm 727.3$	$0.776 \pm 0.048$
Blackbox-Hybrid, linear constraint	<b><math>0.589 \pm 0.070</math></b>	$4849.7 \pm 650.3$	$0.774 \pm 0.040$
SciReN, linear constraint (1-layer KAN)	$0.582 \pm 0.080$	$4708.2 \pm 673.1$	$0.769 \pm 0.049$
SciReN, linear constraint (2-layer KAN)	$0.571 \pm 0.094$	$4707.3 \pm 826.3$	$0.765 \pm 0.052$



useful biases towards simplicity. Most importantly, SciReN is fully transparent – it respects existing scientific knowledge while being able to generate novel insights, thus facilitating data-driven scientific discovery.

### Acknowledgements

This research is supported by AI-LEAF: “AI Institute for Land, Economy, Agriculture, and Forestry”, funded by the USDA National Institute of Food and Agriculture (NIFA) and the NSF National AI Research Institutes Competitive Award. This research is also partially supported by Schmidt Sciences programs, an AI2050 Senior Fellowship and an Eric and Wendy Schmidt AI in Science Postdoctoral Fellowship; the National Science Foundation; the US Department of Energy; the CALS Moonshot Seed Grant program; the “NYS Connects: Climate Smart Farms & Forestry” project, funded by the USDA, the New York State Department of Environmental Conservation, and the New York State Department of Agriculture and Markets; an NSF Research Traineeship (NRT) fellowship in Digital Plant Science; and the Air Force Office of Scientific Research.

### References

- Agarwal, R.; Melnick, L.; Frosst, N.; Zhang, X.; Lengerich, B.; Caruana, R.; and Hinton, G. E. 2021. Neural additive models: Interpretable machine learning with neural nets. *Advances in neural information processing systems*, 34: 4699–4711.
- Apley, D. W.; and Zhu, J. 2020. Visualizing the effects of predictor variables in black box supervised learning models. *Journal of the Royal Statistical Society Series B: Statistical Methodology*, 82(4): 1059–1086.
- Bai, Y.; Chen, D.; and Gomes, C. P. 2021. CLR-DRNets: Curriculum learning with restarts to solve visual combinatorial games. In *27th International Conference on Principles and Practice of Constraint Programming (CP 2021)*, 17–1. Schloss Dagstuhl–Leibniz-Zentrum für Informatik.
- Beuclet, T.; Rasp, S.; Pritchard, M.; and Gentine, P. 2019. Achieving conservation of energy in neural network emulators for climate modeling. *arXiv preprint arXiv:1906.06622*.
- Chen, D.; Bai, Y.; Ament, S.; Zhao, W.; Guevarra, D.; Zhou, L.; Selman, B.; van Dover, R. B.; Gregoire, J. M.; and Gomes, C. P. 2021. Automating crystal-structure phase mapping by combining deep learning with constraint reasoning. *Nature Machine Intelligence*, 3(9): 812–822.
- Chen, D.; Bai, Y.; Zhao, W.; Ament, S.; Gregoire, J.; and Gomes, C. 2020. Deep reasoning networks for unsupervised pattern de-mixing with constraint reasoning. In *International Conference on Machine Learning*, 1500–1509. PMLR.
- Cohrs, K.-H.; Varando, G.; Carvalhais, N.; Reichstein, M.; and Camps-Valls, G. 2024. Causal hybrid modeling with double machine learning—applications in carbon flux modeling. *Machine Learning: Science and Technology*, 5(3): 035021.
- Cuddington, K.; Fortin, M.-J.; Gerber, L.; Hastings, A.; Liebhold, A.; O’connor, M.; and Ray, C. 2013. Process-based models are required to manage ecological systems in a changing world. *Ecosphere*, 4(2): 1–12.
- Daw, A.; Karpatne, A.; Watkins, W. D.; Read, J. S.; and Kumar, V. 2022. Physics-guided neural networks (pgnn): An application in lake temperature modeling. In *Knowledge guided machine learning*, 353–372. Chapman and Hall/CRC.
- Daw, A.; Thomas, R. Q.; Carey, C. C.; Read, J. S.; Appling, A. P.; and Karpatne, A. 2020. Physics-guided architecture (pga) of neural networks for quantifying uncertainty in lake temperature modeling. In *Proceedings of the 2020 siam international conference on data mining*, 532–540. SIAM.
- Dieleman, W. I.; Vicca, S.; Dijkstra, F. A.; Hagedorn, F.; Hovenden, M. J.; Larsen, K. S.; Morgan, J. A.; Volder, A.; Beier, C.; Dukes, J. S.; et al. 2012. Simple additive effects are rare: a quantitative review of plant biomass and soil process responses to combined manipulations of CO<sub>2</sub> and temperature. *Global change biology*, 18(9): 2681–2693.
- Eilers, P. H.; and Marx, B. D. 1996. Flexible smoothing with B-splines and penalties. *Statistical science*, 11(2): 89–121.



- Eilers, P. H.; and Marx, B. D. 2010. Splines, knots, and penalties. *Wiley Interdisciplinary Reviews: Computational Statistics*, 2(6): 637–653.
- Fan, J.; Chen, D.; Wen, J.; Sun, Y.; and Gomes, C. 2022. Monitoring Vegetation From Space at Extremely Fine Resolutions via Coarsely-Supervised Smooth U-Net. In *Proceedings of the Thirty-First International Joint Conference on Artificial Intelligence*, 5066–5072.
- Feng, D.; Liu, J.; Lawson, K.; and Shen, C. 2022. Differentiable, learnable, regionalized process-based models with multiphysical outputs can approach state-of-the-art hydrologic prediction accuracy. *Water Resources Research*, 58(10): e2022WR032404.
- Friedman, J. H. 2001. Greedy function approximation: a gradient boosting machine. *Annals of statistics*, 1189–1232.
- Greenwell, B. M.; Boehmke, B. C.; and McCarthy, A. J. 2018. A simple and effective model-based variable importance measure. *arXiv preprint arXiv:1805.04755*.
- Huang, Y.; Lu, X.; Shi, Z.; Lawrence, D.; Koven, C. D.; Xia, J.; Du, Z.; Kluzek, E.; and Luo, Y. 2018. Matrix approach to land carbon cycle modeling: A case study with the Community Land Model. *Global Change Biology*, 24(3): 1394–1404.
- Jia, X.; Willard, J.; Karpatne, A.; Read, J.; Zwart, J.; Steinbach, M.; and Kumar, V. 2019. Physics guided RNNs for modeling dynamical systems: A case study in simulating lake temperature profiles. In *Proceedings of the 2019 SIAM international conference on data mining*, 558–566. SIAM.
- Jia, X.; Willard, J.; Karpatne, A.; Read, J. S.; Zwart, J. A.; Steinbach, M.; and Kumar, V. 2021. Physics-guided machine learning for scientific discovery: An application in simulating lake temperature profiles. *ACM/IMS Transactions on Data Science*, 2(3): 1–26.
- Jobbágy, E. G.; and Jackson, R. B. 2000. The vertical distribution of soil organic carbon and its relation to climate and vegetation. *Ecological applications*, 10(2): 423–436.
- Karpatne, A.; Jia, X.; and Kumar, V. 2024. Knowledge-guided machine learning: Current trends and future prospects. *arXiv preprint arXiv:2403.15989*.
- Karpatne, A.; Kannan, R.; and Kumar, V. 2022. *Knowledge guided machine learning: Accelerating discovery using scientific knowledge and data*. CRC Press.
- Krishnapriyan, A.; Gholami, A.; Zhe, S.; Kirby, R.; and Mahoney, M. W. 2021. Characterizing possible failure modes in physics-informed neural networks. *Advances in neural information processing systems*, 34: 26548–26560.
- Lal, R.; Negassa, W.; and Lorenz, K. 2015. Carbon sequestration in soil. *Current Opinion in Environmental Sustainability*, 15: 79–86.
- LeCun, Y.; Bengio, Y.; et al. 1995. Convolutional networks for images, speech, and time series. *The handbook of brain theory and neural networks*, 3361(10): 1995.
- Lee, H.; Calvin, K.; Dasgupta, D.; Krinner, G.; Mukherji, A.; Thorne, P.; Trisos, C.; Romero, J.; Aldunce, P.; Barret, K.; et al. 2023. IPCC, 2023: Climate change 2023: Synthesis report, summary for policymakers. Contribution of working groups I, II and III to the sixth assessment report of the intergovernmental panel on climate change [core writing team, h. Lee and j. Romero (eds.)]. IPCC, Geneva, Switzerland.
- Liu, L.; Zhou, W.; Guan, K.; Peng, B.; Xu, S.; Tang, J.; Zhu, Q.; Till, J.; Jia, X.; Jiang, C.; et al. 2024a. Knowledge-guided machine learning can improve carbon cycle quantification in agroecosystems. *Nature communications*, 15(1): 357.
- Liu, Z.; Ma, P.; Wang, Y.; Matusik, W.; and Tegmark, M. 2024b. Kan 2.0: Kolmogorov-arnold networks meet science. *arXiv preprint arXiv:2408.10205*.
- Liu, Z.; Wang, Y.; Vaidya, S.; Ruehle, F.; Halverson, J.; Soljačić, M.; Hou, T. Y.; and Tegmark, M. 2024c. Kan: Kolmogorov-arnold networks. *arXiv preprint arXiv:2404.19756*.
- Lu, X.; Du, Z.; Huang, Y.; Lawrence, D.; Kluzek, E.; Collier, N.; Lombardozzi, D.; Sobhani, N.; Schuur, E. A.; and Luo, Y. 2020. Full implementation of matrix approach to biogeochemistry module of CLM5. *Journal of Advances in Modeling Earth Systems*, 12(11): e2020MS002105.
- Lu, X.; Wang, Y.-P.; Luo, Y.; and Jiang, L. 2018. Ecosystem carbon transit versus turnover times in response to climate warming and rising atmospheric CO<sub>2</sub> concentration. *Biogeosciences*, 15(21): 6559–6572.
- Lundberg, S. M.; and Lee, S.-I. 2017. A unified approach to interpreting model predictions. *Advances in neural information processing systems*, 30.
- Luo, Y.; Ahlström, A.; Allison, S. D.; Batjes, N. H.; Brovkin, V.; Carvalhais, N.; Chappell, A.; Ciais, P.; Davidson, E. A.; Finzi, A.; et al. 2016. Toward more realistic projections of soil carbon dynamics by Earth system models. *Global Biogeochemical Cycles*, 30(1): 40–56.
- Luo, Y.; Huang, Y.; Sierra, C. A.; Xia, J.; Ahlström, A.; Chen, Y.; Hararuk, O.; Hou, E.; Jiang, L.; Liao, C.; et al. 2022. Matrix approach to land carbon cycle modeling. *Journal of Advances in Modeling Earth Systems*, 14(7): e2022MS003008.
- Luo, Y.; and Schuur, E. A. 2020. Model parameterization to represent processes at unresolved scales and changing properties of evolving systems. *Global Change Biology*, 26(3): 1109–1117.
- Luo, Y.; and Smith, B. 2022. *Land carbon cycle modeling: Matrix approach, data assimilation, & ecological forecasting*. CRC Press.
- Marcinkevičs, R.; and Vogt, J. E. 2023. Interpretable and explainable machine learning: A methods-centric overview with concrete examples. *Wiley Interdisciplinary Reviews: Data Mining and Knowledge Discovery*, 13(3): e1493.
- Min, Y.; Chang, M.-C.; Kong, S.; Gregoire, J. M.; van Dover, R. B.; Thompson, M. O.; and Gomes, C. P. 2023. Physically Informed Graph-Based Deep Reasoning Net for Efficient Combinatorial Phase Mapping. In *2023 International Conference on Machine Learning and Applications (ICMLA)*, 392–399. IEEE.
- Molnar, C. 2025. *Interpretable Machine Learning*. 3 edition. ISBN 978-3-911578-03-5.

- Raissi, M.; Perdikaris, P.; and Karniadakis, G. E. 2019. Physics-informed neural networks: A deep learning framework for solving forward and inverse problems involving nonlinear partial differential equations. *Journal of Computational physics*, 378: 686–707.
- Rathore, P.; Lei, W.; Frangella, Z.; Lu, L.; and Udell, M. 2024. Challenges in training PINNs: A loss landscape perspective. *arXiv preprint arXiv:2402.01868*.
- Reichstein, M.; Ahrens, B.; Kraft, B.; Camps-Valls, G.; Carvalhais, N.; Gans, F.; Gentine, P.; and Winkler, A. J. 2022. Combining system modeling and machine learning into hybrid ecosystem modeling. In *Knowledge guided machine learning*, 327–352. Chapman and Hall/CRC.
- Ribeiro, M. T.; Singh, S.; and Guestrin, C. 2016. Model-agnostic interpretability of machine learning. *arXiv preprint arXiv:1606.05386*.
- Rudin, C. 2019. Stop explaining black box machine learning models for high stakes decisions and use interpretable models instead. *Nature machine intelligence*, 1(5): 206–215.
- Shen, C.; Appling, A. P.; Gentine, P.; Bandai, T.; Gupta, H.; Tartakovsky, A.; Baity-Jesi, M.; Fenicia, F.; Kifer, D.; Li, L.; et al. 2023. Differentiable modelling to unify machine learning and physical models for geosciences. *Nature Reviews Earth & Environment*, 4(8): 552–567.
- Sundararajan, M.; Taly, A.; and Yan, Q. 2017. Axiomatic attribution for deep networks. In *International conference on machine learning*, 3319–3328. PMLR.
- Tan, T.; Genova, G.; Heuvelink, G. B.; Lehmann, J.; Poggio, L.; Woolf, D.; and You, F. 2024. Importance of Terrain and Climate for Predicting Soil Organic Carbon Is Highly Variable across Local to Continental Scales. *Environmental science & technology*, 58(26): 11492–11503.
- Tao, F.; Huang, Y.; Hungate, B. A.; Manzoni, S.; Frey, S. D.; Schmidt, M. W. I.; Reichstein, M.; Carvalhais, N.; Ciais, P.; Jiang, L.; et al. 2023. Microbial carbon use efficiency promotes global soil carbon storage. *Nature (London)*, 618(7967).
- Tao, F.; Zhou, Z.; Huang, Y.; Li, Q.; Lu, X.; Ma, S.; Huang, X.; Liang, Y.; Hugelius, G.; Jiang, L.; et al. 2020. Deep learning optimizes data-driven representation of soil organic carbon in earth system model over the conterminous United States. *Frontiers in Big Data*, 3: 17.
- Tsai, W.-P.; Feng, D.; Pan, M.; Beck, H.; Lawson, K.; Yang, Y.; Liu, J.; and Shen, C. 2021. From calibration to parameter learning: Harnessing the scaling effects of big data in geoscientific modeling. *Nature communications*, 12(1): 5988.
- van Bree, R.; Marcos, D.; and Athanasiadis, I. 2025. Hybrid Phenology Modeling for Predicting Temperature Effects on Tree Dormancy. *arXiv preprint arXiv:2501.16848*.
- Wang, S.; Chen, W.; Xie, S. M.; Azzari, G.; and Lobell, D. B. 2020. Weakly supervised deep learning for segmentation of remote sensing imagery. *Remote Sensing*, 12(2): 207.
- Willard, J.; Jia, X.; Xu, S.; Steinbach, M.; and Kumar, V. 2022. Integrating scientific knowledge with machine learning for engineering and environmental systems. *ACM Computing Surveys*, 55(4): 1–37.
- Xu, H.; Fan, J.; Tao, F.; Jiang, L.; You, F.; Houlton, B. Z.; Sun, Y.; Gomes, C. P.; and Luo, Y. 2025. Biogeochemistry-Informed Neural Network (BINN) for Improving Accuracy of Model Prediction and Scientific Understanding of Soil Organic Carbon. *arXiv preprint arXiv:2502.00672*.

## A Technical Appendices

### A.1 KAN edge score computation

We review how we compute edge scores in KAN for sparsity regularization, which is similar to the KAN 2.0 paper (Liu et al. 2024b). Define  $E_{l,i,j}$  as the standard deviation of the activations (outputs) of the  $(l, i \rightarrow j)$  edge (over the BATCH dimension):

$$E_{l,i,j} = \text{Std}(\phi_{l,i,j}(x_{l-1,i})) \quad (18)$$

and  $N_{l,j}$  as the variance of the outputs of node  $(l, j)$ :

$$N_{l,j} = \text{Std}\left(\sum_{i=1}^{n_{l-1}} \phi_{l,i,j}(x_{l-1,i})\right) \quad (19)$$

We now compute node and edge scores iteratively. Start with last layer, and set output node scores  $A_{L,i}$  to be the variance of output  $i$ . Then compute scores as follows for each layer  $l = L, \dots, 1$ :<sup>2</sup>

$$B_{l-1,i,j} = A_{l,j} \frac{E_{l-1,i,j}}{N_{l,j}} \quad (20)$$

$$A_{l-1,i} = \sum_{j=0}^{n_l} B_{l-1,i,j} \quad (21)$$

Intuitively,  $A_{l,j}$  represents how much variance (across all outputs) is contributed by the output of neuron  $(l, j)$ , and  $B_{l,i,j}$  is how much variance is contributed by the output of edge  $(l, i \rightarrow j)$ . For the first equation, we first look at the contribution of neuron  $(l, j)$  towards the final variances, and then split it across the input edges according to the fraction of this neuron’s variance contributed by each incoming edge ( $\frac{E_{l-1,i,j}}{N_{l,j}}$ ). For the second equation, we compute each neuron’s contribution towards the final variances by summing over the contributions via each *outgoing* edge.

### A.2 Ecosystem respiration: data and process-based model

For the ecosystem respiration experiments, we used the process-based model and dataset from (Reichstein et al. 2022). We have labels for output variable  $R_{eco}$  (ecosystem respiration). The process-based model specifies that  $R_{eco}$  is a differentiable function of two latent parameters, base respiration  $R_b$  and temperature sensitivity  $Q_{10}$ . Specifically:

$$R_{eco} = g_{PBM}(\mathbf{p}, \mathbf{x}) = R_b(\mathbf{x}) \cdot Q_{10}^{\frac{t_a - T_{ref}}{10}} \quad (22)$$

where the latent parameters are  $\mathbf{p} = \{R_b, Q_{10}\}$ , the input features are  $\mathbf{x} = \{sw\_pot, dsw\_pot, t_a\}$  (potential shortwave radiation, derivative of potential shortwave radiation, air temperature), and  $T_{ref} = 15$  is a constant. In this example,  $R_b$  is a function of input features, while  $Q_{10}$  is assumed to be independent of the input features and is a global learnable constant.

<sup>2</sup>Eq 9a in KAN 2.0 paper wrote the first equation differently, but I think it must be typos? This is my guess based on intuition and code.

Note that this model is somewhat ill-posed, as the input feature temperature ( $t_a$ ) can influence  $R_{eco}$  either through changing the base respiration  $R_b$ , or through the  $Q_{10}$  exponential term. For example, as explained in (Cohrs et al. 2024), if the model predicted the wrong value of  $Q_{10}$ , it can adjust its predicted  $R_b$  to compensate and still match the labels for  $R_{eco}$ , as follows:

$$R_{eco} = \underbrace{R_b^{TRUE}(\mathbf{x}) \cdot \left(\frac{Q_{10}^{TRUE}}{Q_{10}^{PRED}}\right)^{\frac{t_a - T_{ref}}{10}}}_{\text{Predicted } R_b} \cdot (Q_{10}^{PRED})^{\frac{t_a - T_{ref}}{10}} \quad (23)$$

where the predicted  $R_b$  function soaked up additional temperature dependencies that should have been included in the  $Q_{10}$  exponential. Thus the task is difficult, but SciReN’s bias towards linear and sparse functions can allow it to recover the true  $R_b$ .

The dataset and splits are the same as used in (Reichstein et al. 2022; Cohrs et al. 2024), except that we remove datapoints with top-20%  $t_a$  (temperature) values from the training set (and not the validation/test sets), to test the model’s ability to generalize out-of-distribution. This results in 56102 training, 17520 validation, and 17568 test datapoints. The input features are taken from values observed by a EC tower in Neustift, Austria. The  $Q_{10}$  parameter (latent) was set to 1.5. We created two sets of latent  $R_b$  (base respiration) values:

1. First, we model  $R_b$  as a linear function of 2 features  $sw\_pot, dsw\_pot$  (following (Reichstein et al. 2022)):

$$R_b = 0.0075 \cdot sw\_pot - 0.00375 \cdot dsw\_pot + 1.03506858 \quad (24)$$

where the constant 1.03506858 was selected to make all values non-negative.

2. Second, to create a setting where 2-layer KAN is needed, we add an absolute value.

$$R'_b = 0.0075 \cdot sw\_pot - 0.00375 \cdot dsw\_pot \quad (25)$$

$$R_b = \left| \frac{R'_b - \text{mean}(R'_b)}{\text{stdev}(R'_b)} \right| + 0.1 \quad (26)$$

We then generated the observed variable  $R_{eco}$  according to the process-based model with multiplicative noise, as in (Cohrs et al. 2024):

$$R_{eco} = R_b \cdot Q_{10}^{\frac{t_a - T_{ref}}{10}} \cdot (1 + \epsilon), \quad \epsilon \sim N(0, 0.1), \text{truncated to } [-0.95, 0.95] \quad (27)$$

### A.3 Ecosystem respiration: hyperparameters

We initialized  $Q_{10}$  to 0.5 for all models (so it should increase during training), and give  $Q_{10}$  a learning rate that is 100 times as high as the other learnable parameters in the model. We fixed  $\lambda_{param}$  to 1 if using the ReLU constraint. For PureNN and Blackbox-Hybrid, we used an MLP with 2 layers and 16 hidden units. For SciReN, we used KANs with cubic splines, 30 grid points, and a margin of 2 times the input range.

For each method, we tuned hyperparameters using a grid search, selecting the hyperparameters that had the lowest validation mean-squared-error loss. For Pure-NN and Blackbox-Hybrid, we considered learning rates from  $[10^{-4}, 10^{-3}, 10^{-2}, 10^{-1}]$ , and weight decay from  $[0, 10^{-4}, 10^{-3}]$ . For the KAN-based methods, we considered learning rates from  $[10^{-3}, 10^{-2}, 10^{-1}]$ , weight decay from  $[0, 10^{-4}]$ , and considered  $\lambda_{entropy}, \lambda_{L1}, \lambda_{smooth}$  from  $[10^{-3}, 10^{-2}, 10^{-1}, 1]$ . (We generally set  $\lambda_{entropy} = \lambda_{L1}$ . Due to the number of hyperparameters in KAN, we did not try all configurations.)

The hyperparameters selected for Table 1 (linear  $R_b$ ) are shown below in Table 5. We also report approximate run-times per run on a single V100 GPU.

The hyperparameters selected for Table 2 (nonlinear  $R_b$ ) are shown below in Table 6, along with approximate run-times per run on a single V100 GPU. Note that for 2-layer KAN, we used 8 hidden units, and we used a ‘zero’ base function (instead of identity).

#### A.4 Ecosystem respiration: Additional figures

For Linear  $R_b$  we present additional figures demonstrating the qualitative performance of various methods (Figures 5, 6, 7, 8).

#### A.5 Soil carbon cycle: CLM5 process-based model and datasets

The textbook by Luo and Smith (2022) provides a detailed introduction to land carbon cycle models, but we summarize some key details here. As stated in the main text, we can write the change in carbon for each pool as the difference between inputs and outputs:

$$\frac{dY_i(t)}{dt} = \text{inflow to pool } i - \text{outflow from pool } i \quad (28)$$

Since there are 140 equations (one for each pool), we can stack them into a single matrix equation as follows:

$$\frac{dY(t)}{dt} = B(\mathbf{p}, t)I(t) - A(\mathbf{p}) \text{diag}(\xi(t) \odot K(\mathbf{p})) Y(t) - V(\mathbf{p}, t)Y(t) \quad (29)$$

Here,  $Y(t) \in \mathbb{R}^{140}$  is the amount of carbon in each of the 140 pools at time  $t$ .  $I(t) \in \mathbb{R}$  is the total carbon input to the system from vegetation at time  $t$ , and  $B(t) \in \mathbb{R}^{140}$  is the allocation of input to different pools.  $A(\mathbf{p}, t) \in \mathbb{R}^{140 \times 140}$  quantifies carbon transfers between pools at the same depth.  $K(\mathbf{p}) \in \mathbb{R}^{140}$  contains the intrinsic decomposition rate of each carbon pool, which is the same for each pool across 20 layers.  $\xi(t) \in \mathbb{R}^{140}$  is computed based on monthly climate data and indicates how the environment modifies the intrinsic decomposition rate.  $\xi$  and  $K$  are multiplied elementwise and then converted into a  $140 \times 140$  diagonal matrix.  $V(\mathbf{p}, t) \in \mathbb{R}^{140 \times 140}$  quantifies vertical carbon transfers between adjacent depths.  $\odot$  denotes elementwise multiplication, while  $\text{diag}$  indicates we construct a diagonal matrix from the given vector. The  $t$  indicates that the parameter varies with time, while  $\mathbf{p}$  indicates that the matrix is constructed in a deterministic way from latent biogeochemical

parameters predicted by the encoder. In this study we do not consider temporal variations, but any parameters that depend on  $t$  are constructed using *monthly-average* climate forcing data.

In this work, we assume steady state ( $\frac{dY}{dt} = 0$ ), which is a reasonable assumption since previous research has shown that recent disequilibrium effects from climate change and human activities are minor in comparison to the total SOC storage that has developed over thousands of years (Tao et al. 2023; Lu et al. 2018). Thus, we can solve for  $Y$  analytically as a function of  $\mathbf{p}$ :

$$\hat{Y}(t) = [A(\mathbf{p}) \text{diag}(\xi(t) \odot K(\mathbf{p})) + V(\mathbf{p}, t)]^{-1} B(\mathbf{p}, t)I(t)$$

Note that  $\hat{Y}(t)$  contains predicted carbon amounts at 20 fixed layers, and 7 pools per layer. However, our labels are only aggregate SOC amounts at specific depths (which may not match the 20 fixed layers). Thus, we sum up the SOC pools at each layer, and linearly interpolate to predict SOC at the observed depths.

The datasets used in these experiments are documented in (Tao et al. 2020; Xu et al. 2025). We restricted to ten input features for interpretability:

1. Annual mean temperature
2. Annual precipitation
3. Clay content
4. Sand content
5. Bulk density
6. Soil water capacity
7. Soil pH in H2O
8. Cation Exchange Capacity
9. NPP (Net Primary Productivity)
10. Vegetation Carbon Stock

To test SciReN’s ability on small datasets, we only use 1018 examples in our dataset total, which are representative locations in the conterminous United States. We split the dataset spatially into  $2 \times 2$ -degree blocks, and assign each block to one of 5 folds. We run experiments across 5 splits, each time holding out a different test fold (and validation fold).

For the synthetic functional relationship experiment, we only considered the four most sensitive biogeochemical parameters identified in (Xu et al. 2025), as the other parameters are poorly constrained by data. We randomly selected 20% of the possible input-output relationships to exist. For each relationship, we randomly draw a function (linear, quadratic, exponential, logarithmic, absolute value), and add random affine shifts. We then calculate the value of each output parameter as the sum of functions of each relevant input, e.g.

$$p_i = f_{i,2}(x_2) + f_{i,6}(x_6) = \log(ax_2 + b) + (cx_6^2 + d) \quad (30)$$

An example of the true prescribed functional relationships is shown in Figure 9.

Table 5: Hyperparameters for Table 1.

Method	LR	Weight decay	$\lambda_{entropy}, \lambda_{L1}$	$\lambda_{smooth}$	Runtime
Pure-NN	0.1	0	-	-	15min
Blackbox-Hybrid, nonlinear constraint	0.1	0	-	-	24min
Blackbox-Hybrid, linear constraint	0.1	0	-	-	24min
SciReN, nonlinear constraint (1-layer KAN)	0.1	$10^{-4}$	0.01	0.1	15min
SciReN, linear constraint (1-layer KAN)	0.01	$10^{-4}$	0.01	1.0	15min

Table 6: Hyperparameters for Table 2.

Method	LR	Weight decay	$\lambda_{entropy}, \lambda_{L1}$	$\lambda_{smooth}$	Runtime
Pure-NN	0.1	0	-	-	25min
Blackbox-Hybrid, nonlinear constraint	$10^{-3}$	$10^{-3}$	-	-	25min
Blackbox-Hybrid, linear constraint	$10^{-3}$	$10^{-4}$	-	-	25min
SciReN, linear constraint (1-layer KAN)	0.1	$10^{-4}$	0.01	0.1	20min
SciReN, linear constraint (2-layer KAN)	0.01	$10^{-4}$	$10^{-3}$	1.0	38min

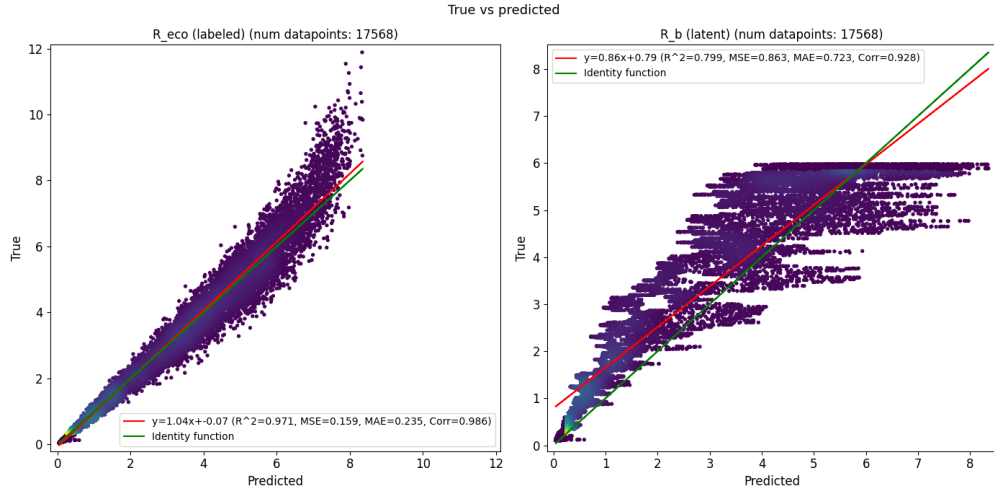


Figure 5: Pure NN (Table 1, linear  $R_b$ ). Because the model does not have access to scientific knowledge (process-based model), it struggles to extrapolate on the higher end of ecosystem respiration / temperature (left). It is also unable to predict the latent variable (right).

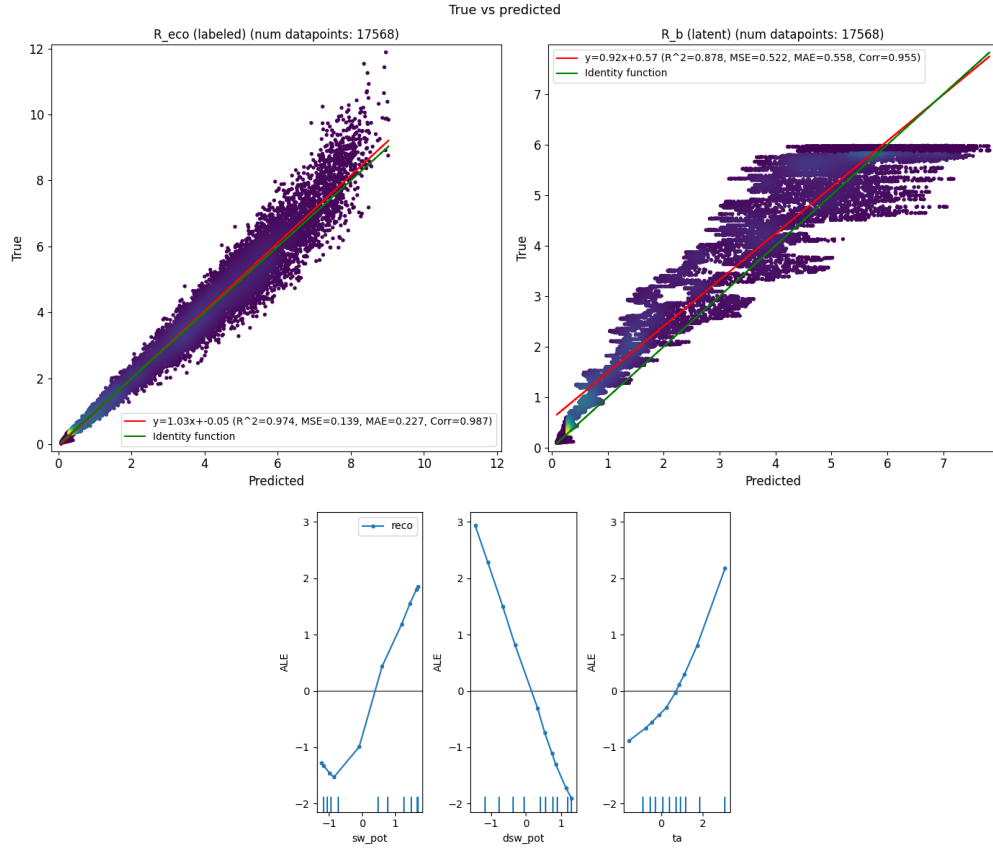


Figure 6: Blackbox-Hybrid, nonlinear constraint (Table 1, linear  $R_b$ ). The process-based model helps with extrapolation (top left). However the latent variable prediction is inaccurate (top right). According to the Accumulated Local Effects plots (which estimate the impact of each input feature; bottom), the model thinks that both  $sw\_pot$  and  $t_a$  influence the latent variable, but only  $sw\_pot$  is actually relevant.

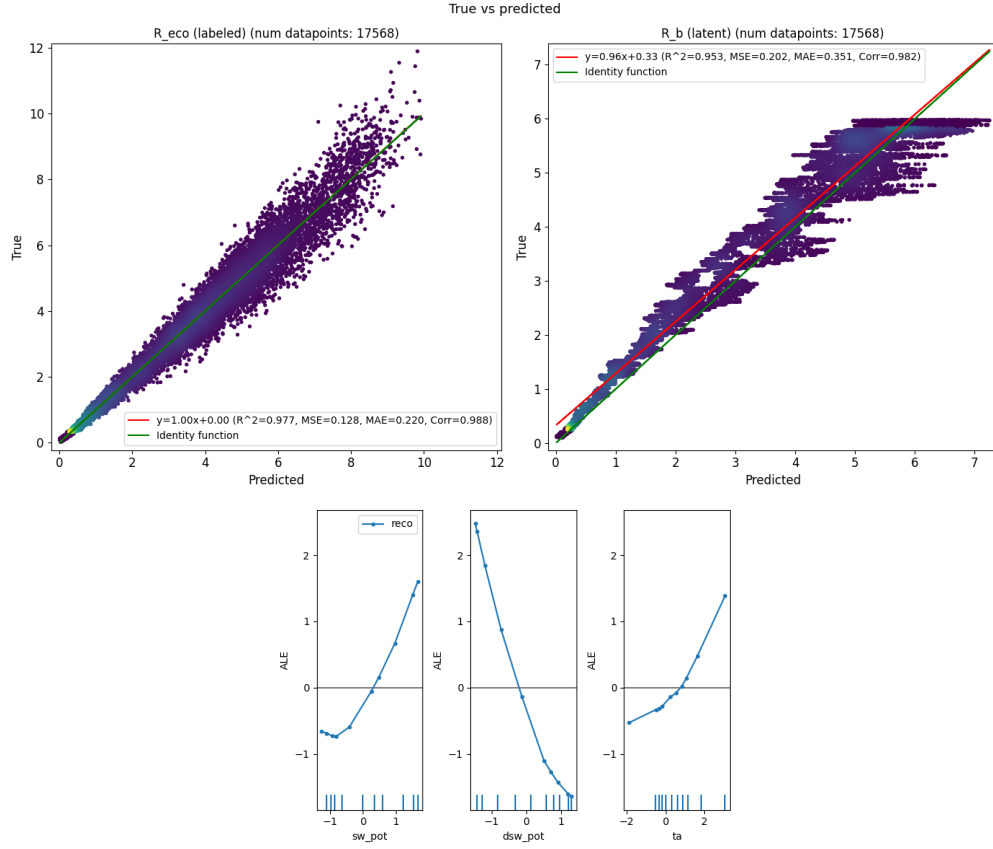


Figure 7: Blackbox-Hybrid, linear constraint (Table 1, linear  $R_b$ ). Changing to linear constraint improves the latent variable prediction (top right) since the model now only needs to learn a simple linear relationship between  $R_b$  and input features. However, the model is still using  $t_a$  somewhat even though it is actually useless (bottom).



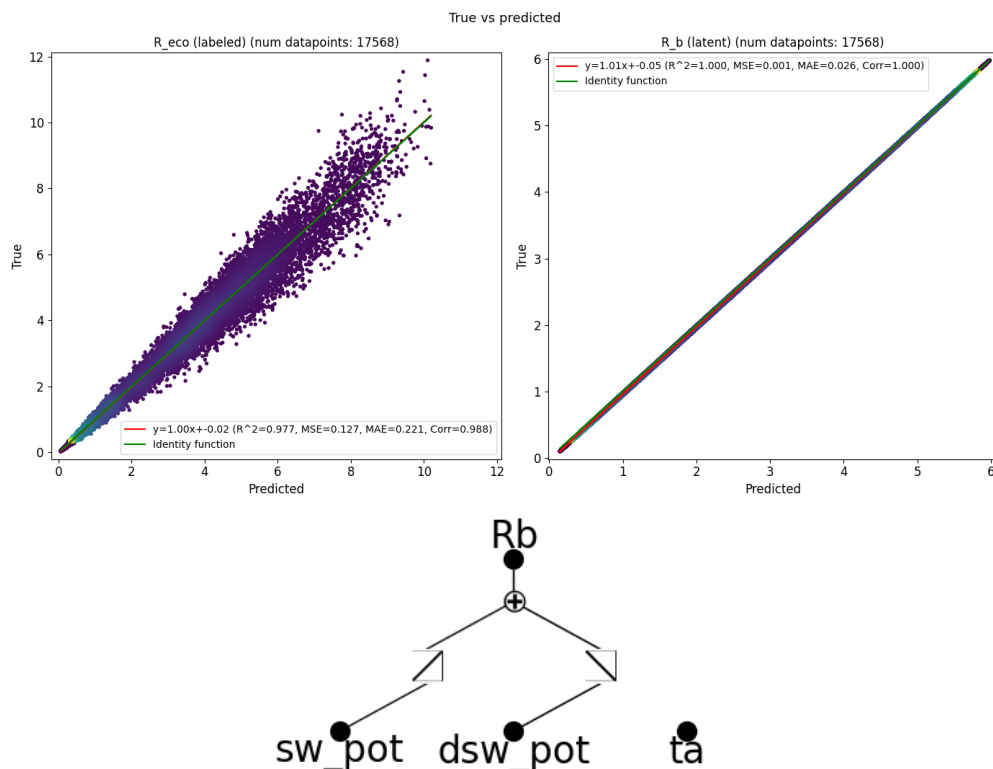


Figure 8: SciReN, linear constraint (Table 1, linear  $R_b$ ). SciReN's entropy loss encourages sparsity, forcing it to choose the best among correlated features. The smoothness loss also encourages a near-linear function. Thus, it is able to predict the observed variable (top left), latent variable (top right), and functional relationships (bottom) correctly.

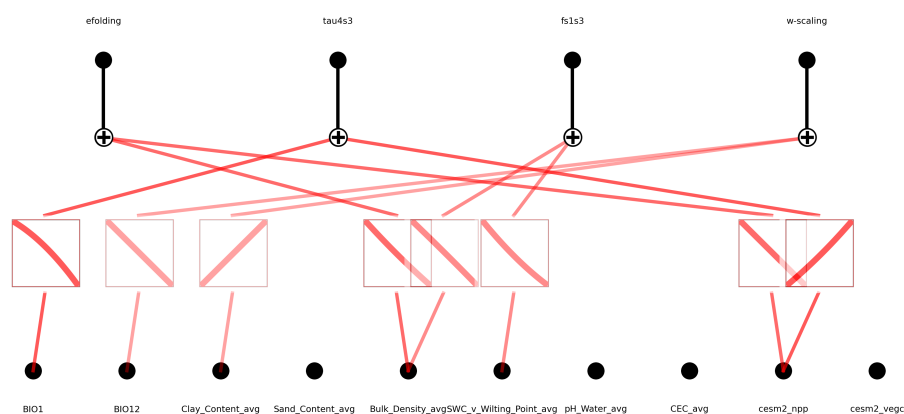


Figure 9: Prescribed functional relationships.

## A.6 Soil carbon cycle: Hyperparameters

For soil carbon cycle: for neural networks, we used a 3-layer MLP with 128 hidden units, residual connection, batch normalization, and leaky ReLU activation. We set the temperature  $\tau = 1$ . For KANs, we used cubic splines, 30 grid points, and a margin of 2 times the input range; we also used 128 hidden units for the 2-layer KAN (probably too many). We set  $\lambda_{param} = 1000$  if using hardsigmoid (linear constraint).

We tuned the learning rate from  $[10^{-4}, 10^{-3}, 10^{-2}, 10^{-1}]$ , weight decay from  $[0, 10^{-4}, 10^{-3}]$ ,  $\lambda_{entropy}, \lambda_{L1}$  from  $[0.1, 1, 10]$ , and  $\lambda_{smooth}$  from  $[10, 100, 1000]$ . The weights are higher than for ecosystem respiration because the magnitude of the supervised loss is 100-1000 times larger.

Table 7 contains hyperparameters used for Table 3. These were trained using a single CPU.

Table 8 contains hyperparameters used for Table 4. These were trained using PyTorch DistributedDataParallel on 8 CPUs.

## A.7 Computational Resources

For ecosystem respiration, experiments were run on a cluster, using a single NVIDIA V100 GPU. For CLM5, experiments were run on a cluster using 1 or 8 CPUs (no GPUs). (For the synthetic experiment in Table 3, using 1 CPU performed better than 8 CPUs, possibly because distributed training with 8 CPUs made it hard for each worker’s gradient updates to agree on which connections to choose.) For the real label experiments used 8 CPUs with distributed training. Some runs were also performed on a laptop with M3 chip.

We did not log the total amount of compute required for all failed experiments. The total amount of cluster usage during this period was about 17,000 CPU-hours; this included a small amount of time spent on other projects, but excluded runs on a local laptop, which may be roughly equivalent.

## A.8 Ablations

To justify the components of SciReN, in Table 9 we show the results of removing each loss term, on Table 2 (ecosystem respiration, nonlinear  $R_b$ , 2-layer KAN)

Most methods do similarly on the observed variable. On the latent variable, removing L1 (absolute deviation) loss actually did slightly better; the L1 loss and entropy loss are somewhat interchangeable as they both aim to shrink the variance explained by most features to zero. In predicting functional relationships, all losses seem quite valuable. Removing the entropy loss caused a large drop in performance, as the model would pay too much attention to correlated features instead of the true causal one. Finally, reducing to 3 grid cells makes it impossible for the network to learn sharp transitions like the absolute value function.

Table 7: Hyperparameters for Table 3.

Method	LR	Weight decay	$\lambda_{entropy}, \lambda_{L1}$	$\lambda_{smooth}$	Runtime
Pure-NN	$10^{-3}$	0	-	-	15min
Blackbox-Hybrid, nonlinear constraint	$10^{-4}$	$10^{-4}$	-	-	180min
Blackbox-Hybrid, linear constraint	$10^{-3}$	$10^{-4}$	-	-	180min
SciReN, linear constraint (1-layer KAN)	$10^{-2}$	0	10	100	190min

Table 8: Hyperparameters for Table 4.

Method	LR	Weight decay	$\lambda_{entropy}, \lambda_{L1}$	$\lambda_{smooth}$	Runtime
Pure-NN	0.1	0	-	-	2min
Blackbox-Hybrid, nonlinear constraint	$10^{-3}$	0	-	-	25min
Blackbox-Hybrid, linear constraint	$10^{-2}$	$10^{-4}$	-	-	25min
SciReN, linear constraint (1-layer KAN)	$10^{-2}$	0	1	100	40min
SciReN, linear constraint (2-layer KAN)	$10^{-2}$	0	1	100	80min

Table 9: Ecosystem respiration, nonlinear  $R_b$ . Ablations.

Method	$R^2$ (observed, $\uparrow$ )	$R^2$ (latent, $\uparrow$ )	KL, functional relationships ( $\downarrow$ )
Original	<b>0.9619</b>	0.9989	<b>0.1490</b>
Remove smoothness loss	0.9600	0.9720	0.4973
Remove L1 (absolute deviation) loss	0.9618	<b>0.9993</b>	0.2016
Remove entropy loss	0.9608	0.8754	0.6132
Reduce to 3 grid cells	0.9558	0.9863	0.8942